Thermomechanical Behavior of a Wide Slab-Casting Mold

Gavin J. Hamilton, Lance C. Hibbeler, and Brian G. Thomas

The University of Illinois at Urbana–Champaign
Department of Mechanical Science and Engineering
1206 West Green Street (MC 244), Urbana, Illinois, USA, 61801-2906
Phone: +1-217-333-6919 (B. G. Thomas)
Email: ghamilt2@illinois.edu, lhibbel2@illinois.edu, bgthomas@illinois.edu

Keywords: mold distortion, wide slab casting, continuous casting

ABSTRACT

The thermomechanical behavior of a wide slab casting mold is studied using a three dimensional, finite-element model of the mold plates, waterboxes, stiffeners, and tie rods. The thermal model reveals the hot face temperature variations due to the water channel geometry around the bolts and at mold exit. The distortion of the narrow face is reduced greatly by a stiffener plate. The distortions of about 1 mm are on the order of the applied tapers and must be considered when designing taper practice.

1. INTRODUCTION

Continuous casting molds experience thermal distortion, caused by the temperature gradients in the constrained mold that arise during operation. This distortion affects cast product quality and mold life. The magnitude of the distortion typically is on the order of 1 mm, which is small compared to the mold itself but large compared to the size of the strand-mold gap, and therefore must be understood and accommodated when designing caster operating practices. Mold distortion can contribute to strand defects such as longitudinal corner cracking and breakouts.[1]

The thermomechanical behavior of continuous casting molds has been investigated for square[1–4] and round[5–7] billet molds, thick-slab molds,[8–10] thin-slab molds with[11–13] and without a funnel,[12,13] and beam-blank molds.[14] This article focuses on the thermomechanical behavior of a wide slab casting mold, whose geometry is presented in Section 2. Section 3 describes the computational model used to analyze the behavior of the mold and waterbox, and Sections 4 and 5 present the thermal and mechanical results of the numerical model.

The thermal and mechanical behavior of the mold have been calculated as part of multiphysics models that also analyze fluid flow and solidification in the strand,[5,6,15] shell deformation,[5,6] with simplified[15] and fully-coupled[5,6] gap physics. The distortion of the mold changes the size of the strand-mold gap, and consequently changes the heat removal by the mold.[5,12] The mechanical behavior of the mold is insensitive to the details of the molten steel flow, as seen by comparing multiphysics model predictions with laminar[5] and turbulent[6] flow.

1.1. Mold Thermal Behavior

The mechanical behavior of the mold is driven by its thermal behavior. Previous researchers have identified that distortion and/or stress increases with increasing mold temperatures[1,13] or the process variables that cause it, like increasing casting speed,[6] decreasing cooling water speed,[1] and other variables that are not reviewed here.

The general thermal behavior of a continuous casting mold is explained with a one-dimensional model of steady heat conduction.

The hot face temperature T_{hot} is predicted as

$$T_{\text{hot}} = T_{\text{water}} + q_{\text{hot}} \left(\frac{1}{h_{\text{cold}}} + \frac{d_{\text{mold}}}{k_{\text{mold}}} + \frac{d_{\text{coat}}}{k_{\text{coat}}} \right), \tag{1}$$

where T_{water} is the bulk water temperature, q_{hot} is the hot face heat flux, h_{cold} is the effective cold face heat transfer coefficient (HTC) that depends on the cooling water HTC h_{water}, d_{mold} and k_{mold} are the thickness and the thermal conductivity of the mold plate, and d_{coat} and k_{coat} are the thickness and the thermal conductivity of the coating layer. Equation (1) and previous studies show that the hot face temperature increases with increasing plate thickness and decreasing thermal conductivity; changing the plate thickness has a stronger effect than changing the mold material, *i.e.*, the thermal conductivity, for typical alloys.[3,9]

The highest mold temperature is found on the hot face at[8] or a few centimeters below[2,9,12] the meniscus. This region of the mold is particularly susceptible to failure because the highest temperatures correspond to the most expansion, the lowest strength, and the highest creep rates.

Increasing the water channel depth reduces the hot face temperatures, but doing so also increases the temperature and stress at the channel roots,[8] increasing the likelihood of boiling the cooling water and forming a fouling layer. The onset of boiling in the channels increases the mold temperatures and corresponding distortion.[4] Fouling layers in the water channels reduce h_{cold} and the total heat removal, increasing mold temperatures.[13] The thickest fouling deposits are observed a few centimeters below the meniscus.[13] Uneven cooling among the water channels promotes the formation of mold cracks[16] and longitudinal cracks on the strand;[17] such uneven cooling can be caused by locally thicker fouling layers,[17] uneven distribution of water from the waterbox,[17] or by dirt or other impurities clogging a channel.[16] Good plant practice includes filtering the cooling water[16] and periodically inspecting and cleaning any fouling material.[17]

Increasing the cooling water speed, and therefore increasing h_{water} and h_{cold}, decreases the mold temperatures. Restrictor plates have been used to increase the water speed near the meniscus in a slab mold,[17] and along the entire channel length in a beam-blank mold.[18] Another method to reduce mold temperatures is to add small circular channels between larger circular channels, which has been implemented on slab[17] and beam-blank[18] molds. Redesigning the cooling channels must be done carefully: a recent study[14] reduced the hot spot at the shoulder of a beam-blank mold but increased everywhere the hot face temperature, reducing the fatigue life of the mold but reportedly increasing the product quality.

The mold experiences large-amplitude low-frequency temperature cycles of about 300 °C at 0.5×10^{-6} Hz because of startup and shutdown[2] and nozzle changes;[15,19] and low-amplitude high-frequency temperature cycles of about of about 30 °C at 0.5 Hz because of top-surface level fluctuations,[1,2,8,9,15,19] mold oscillations,[1] intermittent boiling in the water channels,[1] and variations in the strand-mold interface[1] caused by, for example, uneven slag melting. These cyclic behaviors drive the fatigue response of the mold.

1.2. Mold Mechanical Behavior

The mold tends to expand nonuniformly as it is heated from room temperature; the constraint provided by the cold side of the mold[2,11,12] and the mold bolts and waterbox[14,15] limits the expansion and forces the mold into compression. The largest stresses usually are sufficient to cause yielding,[1,2,8,9,15] albeit in limited localized areas,[2] though yielding depends on the mold alloy. Shear stresses usually are small compared to normal stresses.[15] Because of the high creep rates and oversized bolt holes in the waterbox that allow motion, the compressive stress relaxes over the course of a casting sequence: for example, the hot face nearly becomes stress-free by the end of a sequence.[15] When the mold temperature drops, because of the end of a sequence or a nozzle change, the corresponding thermal contraction forces the hot face into residual tension and can cause longitudinal cracks just below meniscus.[14,15]

The mold bends into the solidifying steel for most of the length of the mold,[10,12] and bends away from the solidifying steel within a few millimeters of the meniscus and mold exit, particularly for billet molds.[1,5–7] The change in the character of distortion near mold exit is due to changes in the cooling channels in slab[8,10,12] and funnel[11] molds and the lack of constraint[1] or improper taper[5] in billet molds. The NF mold distorts into a somewhat-parabolic arc,[12] like a bimetallic strip, while the WF mold shape is much more complicated. The largest distortion in a constrained mold occurs a few centimeters below the meniscus; experience varies whether the location of highest hot face temperature corresponds to the largest stress[9,14,15] or the largest distortion.[1,5–8,12,15] The largest residual distortion measured on a cold mold after several heats occurs at nearly the same location.[1,4]

The mold constraint is key to controlling the mold distortion.[1] Oversizing the bolt holes to allow lateral motion reduces

overconstraint.[12,15] Operating with the mold level near a point of constraint, like a row of bolts, reduces the most severe distortion but causes larger stresses,[1] and can have a negative influence on mold life.

Thinner mold plates have less distortion, mostly because of the corresponding lower temperature.[8,9,12] This lower temperature and less distortion on thinner plates correspondingly increases the mold life because the fatiguing of the meniscus region is less severe.[15] However, thinner mold plates may lead to higher heat flux and lower slab quality.[13]

Keeping the mold elastic or nearly so during operation has been demonstrated in computational models and plant experience by using a combination of thin mold plates and an alloy with high yield strength and high thermal conductivity;[9] deeper water channels with restrictor plates;[17] and changing the mold taper and improving waterbox manufactuing.[4]

1.3. Clamping Forces

Four-piece molds typically are clamped together with "tie rods" or "pull rods." The clamping forces resist the ferrostatic pressure p_f, which increases with vertical distance below the top of the mold z as

$$p_f = \begin{cases} 0 & \text{if } z \le z_{men} \\ \rho_{steel} g\,(z - z_{men}) & \text{if } z \ge z_{men} \end{cases} \tag{2}$$

where ρ_{steel} is the mass density of the liquid steel, z_{men} is the position of the meniscus below the top of the mold, and g is the gravitational acceleration. The resultant force of the ferrostatic pressure in a slab mold is

$$\begin{aligned} F_f &= \int_0^{\ell_{mold}} \int_{-w_{strand}/2}^{w_{strand}/2} p_f \,dy\,dz \\ &= \frac{1}{2}\rho_{steel} g\left(\ell_{mold}^2 - z_{men}^2\right) w_{strand}, \end{aligned} \tag{3}$$

which acts at $z_{F_f} = \frac{1}{3}z_{men} + \frac{2}{3}\ell_{mold}$ below the top of the mold of length ℓ_{mold}. The clamping forces necessary for static equilibrium, with two tie rods at z_{top} and two more tie rods at z_{bot} below the top of the mold, are

$$2F_{top} = \frac{z_{bot} - z_{F_f}}{z_{bot} - z_{top}} F_f \tag{4}$$

$$2F_{bot} = \frac{z_{F_f} - z_{top}}{z_{bot} - z_{top}} F_f. \tag{5}$$

A free-body diagram of these forces on the mold is shown in Figure 1. If the foot rolls are attached to the mold, the clamping forces also must sustain the ferrostatic pressure transmitted to the foot rolls, which are not shown in Figure 1, in which case the value of ℓ_{mold} used in these calculations should be from the top of the mold to somewhere between the last roll supported by the mold and the first roll that is supported separately by the first segment.

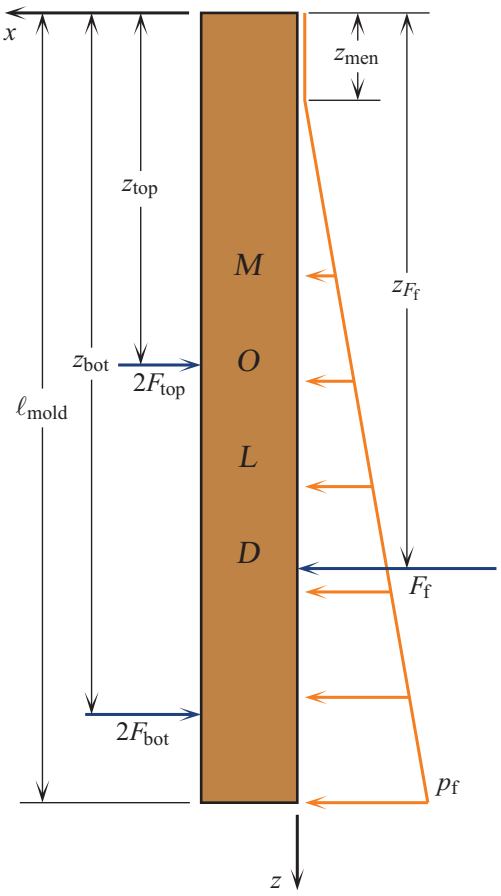

Figure 1. Ferrostatic and clamping forces

The applied clamping forces must exceed the values given by Equations (4) and (5) to hold the mold together, but not so much as to damage the corners of the narrow faces during operation.[17] The resultant force of the ferrostatic pressure increases linearly with slab width, and the applied clamping forces should accommodate this effect;[17] reducing the clamping force for narrower slabs has been shown to increase mold life.[17]

1.4. The Wide Face – Narrow Face Interface

During operation, the broad and narrow faces pivot around each other,[10,15] creating a gap that depends on mold geometry and process conditions. In conventional slab[10] and funnel[11,12,15] molds, calculations show the gap between the cold edge of NF mold and the WF mold is about 1 mm during casting, and grows to about 2 mm after cooling because of stress relaxation.[15] This ability to pivot at the NF corner is the main difference between single-piece and four-piece molds.[10] In beam blank molds, the same pivoting occurs[14] but the gap is about 0.06 mm.

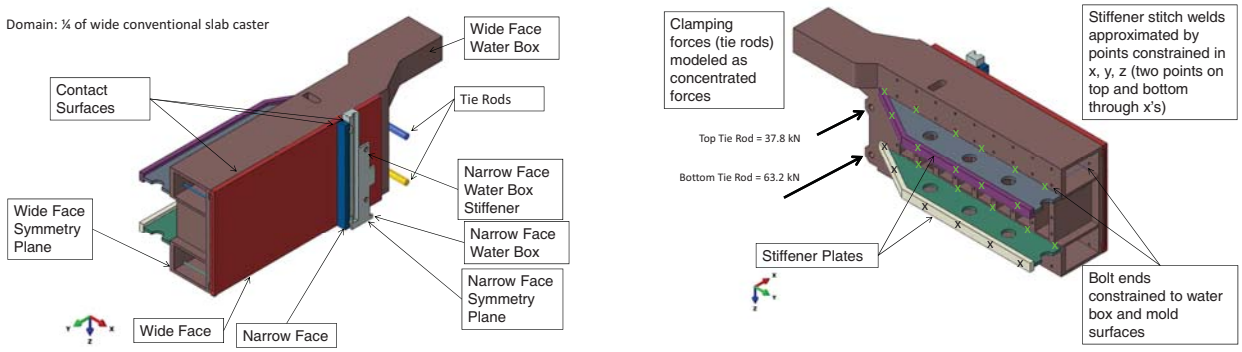

Figure 2. Front and back views of mold assembly, and explanation of boundary conditions

Figure 3. Wide Face Mold Channel Geometry

The molds expand into each other during operation, building contact pressure between the mold plates and inelastically crushing the NF mold corners; over time, the contact stresses relax, and the mold permanently shrinks when cooled.[12,17] During the following heating cycle the WF-NF interface has gaps into which the molten steel can flow and solidify as a sharp fin.[17] The higher expansion near the meniscus and these fin defects can scratch the surface of the wide face mold, exacerbating the problem;[17] too large of a WF-NF gap leads to sticker breakouts.[17]

2. MOLD GEOMETRY

The geometry of the mold plates and waterboxes of the wide slab caster considered in this work is shown in Figure 2. The wide face mold has a length of 904 mm, a width of 3350 mm, and a nominal thickness of 42 mm. The narrow face has a length of 904 mm, a nominal width of 158 mm. The thickness of each wide face mold increases to 42.5 mm and of each narrow face mold decreases to 157 mm at mold exit to implement a linear 0.5 mm per-side wide-face taper. The ball-end-milled water channels are 848 mm long, 5 mm wide, and 22 mm deep on both the narrow and wide faces; the channels are set in banks of 9 between bolt columns at 20.89 mm pitch on the wide face and in a bank of 5 at 17.272 mm pitch on the narrow face. The narrow face mold also has two 9.525 mm diameter bores for water near the corners of the mold.

Each wide face mold is bolted to its waterbox with 126 bolts, arranged in a rectangular array of 7 rows with 136 mm spacing and 18 columns with 188 mm spacing. Each narrow face mold is bolted to its waterbox with 16 bolts, arranged in a rectangular array of 8 rows with 90 mm to 130 mm spacing and 2 columns with 81 mm spacing. The thermocouples are set in two rows of 22, at 275 mm and 475 mm below the top of the mold, with pitch in the range 104.44 mm to 167.11 mm. The water channels slalom around the bolt and thermocouple holes, as seen in Figure 3.

Two stiffeners are welded to the back of the WF water box by 9 stitch welds. Each WF stiffener is built up from two pieces, again stitch-welded together. The narrow face water box is 956 mm tall, and has a 30 mm thick plate that runs along its lower 640 mm to provide additional stiffness.

Only one fourth of the mold assembly is modeled because it is almost symmetrical. The modeled assembly consists of the WF

Table I. Material properties

Part	Material	Mass density kg/m^3	Thermal conductivity W/(m·K)	Thermal expansion coefficient (μm/m)/K	Young's modulus GPa	Poisson's ratio –	Tensile yield strength MPa
Molds	UNS C18150	8890	200	16.5	117.2	0.181	380
Waterbox	SAE 316Ti	8000			200	0.299	220
Wide Face Bolts	SAE A286	7920			201		600
Narrow Face Bolts	SAE A4-70	7990			193		450

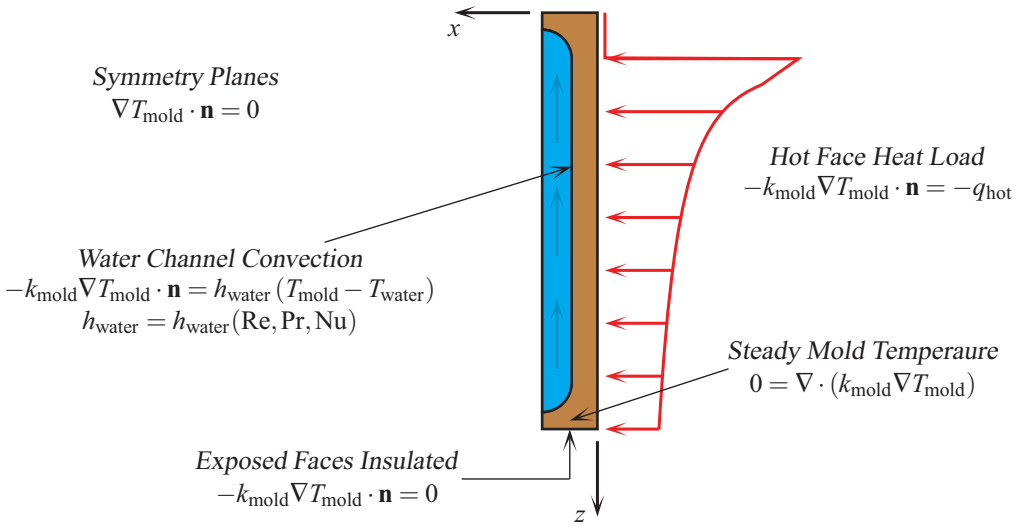

Figure 4. Boundary-value problem for mold plate temperature fields

and NF mold plates and waterboxes, 63 identical WF bolts, and 8 identical NF bolts. The effect of the tie rods is included in the assembly as concentrated forces, reflecting the force-control control system used in the plant. The WF waterbox consists of the main frame and two stiffeners, each of two parts. A Python script was developed to programmatically generate the entire model in the ABAQUS/CAE environment, to reduce model development time and to facilitate a future parametric study of mold geometry. The exact mold and waterbox geometry was included, except for small features unimportant to the distortion.

3. MODEL DESCRIPTION

This section describes the numerical model used to investigate the thermomechanical behavior of a wide slab-casting mold. Mold distortion is a three-dimensional (3D) phenomenon because the temperature gradients through the mold cause nonuniform bending about both planar directions of the mold plate. Two-dimensional (2D) models can be used for quick estimates of the mold behavior,[1,2] but the coarse-mesh 3D models used decades ago are better-suited for quick estimates on modern computing platforms. Mold distortion has been modeled at steady state in two[1,5,7,13,15] and three[1,2,7–13,15] dimensions. These models have used four-fold[8–15] or eight-fold[1,2] symmetry, and a typical longitudinal section of a few channels[10,12] to reduce computational effort. Previous 2D models have analyzed a longitudinal plane with plate elements,[1] and transverse planes in plane strain,[13–15] in plane stress,[1] or unreported out-of-plane behavior,[7] with order-of-magnitude different predictions of distortion resulting from the different assumptions. Round billet molds have been modeled as axisymmetric.[5–7]

3.1. Thermal Model

The temperature field $T_{\text{mold}}(\mathbf{x})$ in each mold piece is the solution of the boundary-value problem described in Figure 4. The mold water is assumed to remove all heat input to the mold, so the thermally-inert waterbox is not included in the thermal analysis. This boundary-value problem is solved most commonly with the finite element method; the finite difference method has found occasional use.[6,20] This work uses the finite element method, implemented in the commercial software ABAQUS. This work is concerned with the steady-state behavior of the mold; note that the high-frequency temperature cycles discussed in Section 1.1 occur quickly enough that steady-state is not achieved, and so must be analyzed with a transient model.[2]

The exposed faces of the mold have been modeled as insulated,[2,8,11–13] with a small heat transfer coefficient,[5,6,15] or unreported;[7,14] in this work the exposed faces are insulated. The convection effect of the mold water typically has been modeled with a heat transfer coefficient from an empirical correlation on the Reynolds, Prandtl, and Nusselt numbers of the flowing water; this approach is adopted in this work. The water channel slaloms around the bolt and thermocouple holes are assumed to not affect significantly the behavior of the cooling water. The interface between the wide and narrow face mold plates is taken as insulated because a large air gap opens at this interface, as discussed in Section 1.4. These assumptions on behavior of the WF-NF interface and of the waterbox allow a one-way coupling where the mold temperature affects the distortion, but the distortion does not affect the mold temperature. This modeling approach incorrectly has been called "uncoupled" in the literature.[2]

The spatial variation of the hot face heat flux q_{hot} and the water heat transfer coefficient h_{water} and bulk temperature T_{water} in this work are calculated with CON1D,[21] a one-dimensional model of heat transfer in the continuous casting of steel. Some of the process parameters used in the calibration are summarized in Table II. The calibrated profiles of these variables are given in Figure 5; the same values are used on both the wide face and narrow face molds. These profiles are input to the model as tabular data and spatially interpolated in the ABAQUS user subroutines `DFLUX` for the heat flux and `FILM` for the heat transfer coefficient and water temperature. Others have obtained the heat flux profile by inverse calculations to match thermocouple measurements.[7,12] Another approach is to adjust the coefficients in a previously-used functional form[8] to specify an average heat removal; this technique must be done carefully because heat flux data from one mold is not appropriate to use in another mold.[5]

Table II. Process parameters

Parameter	Value	Unit
Casting speed	1.092	m/min
Mold level position	100	mm
Steel pour temperature	1532	°C
Steel liquidus temperature	1512	°C
Slab width	2464	mm
Slab thickness	158	mm

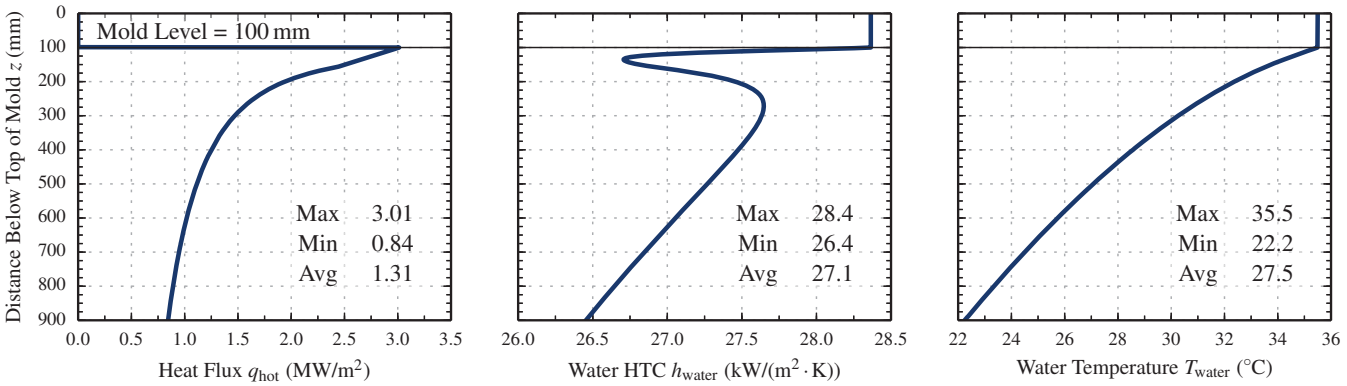

Figure 5. Thermal boundary conditions from CON1D

3.2. Mechanical Model

The displacement vector field $\mathbf{u}(\mathbf{x})$ in the mold assembly is the solution of the boundary-value problem described in Figure 6, which uses the traction vector $\mathbf{t} = \boldsymbol{\sigma}^{\text{T}} \cdot \mathbf{n}$ expressed in terms of the surface normal $\mathbf{n}$ and the Cauchy stress tensor $\boldsymbol{\sigma}$. The mold temperature field calculated with the model described in Section 3.1 drives the mechanical behavior of the mold and waterbox. This work includes the effect of gravity, though it may be neglected because the bolt shear caused by the mold weight is small relative to the bolt pre-stresses,[10] which is discussed further in Section 3.3. The details of some of the boundary conditions are given in Figure 2. This boundary-value problem has been solved exclusively with the finite element method, as is done in this work using the commercial software ABAQUS.

The "active" hot face of the molds are supplied a traction to include the effect of ferrostatic pressure, where the applied pressure p_{f} is described in Section 1.3. The ferrostatic pressure is applied in this work with the ABAQUS user subroutine `DLOAD`. The clamping forces are applied as point forces where the tie rods are mounted to the waterbox, which has been done in previous work.[10,12]

Contacting surfaces between the mold and waterbox and between the WF and NF molds move together or form gaps according to Coulomb friction, based on the relative distance $\mathbf{x}_{\text{rel}}$ and velocity $\mathbf{v}_{\text{rel}}$ of the interacting surfaces with coefficient of friction μ. The copper-copper coefficient of friction is 1.6 and the copper-steel coefficient of friction is 0.53.

The two carrier points on the narrow face stiffener are constrained in the direction towards the SEN, and the top point also is

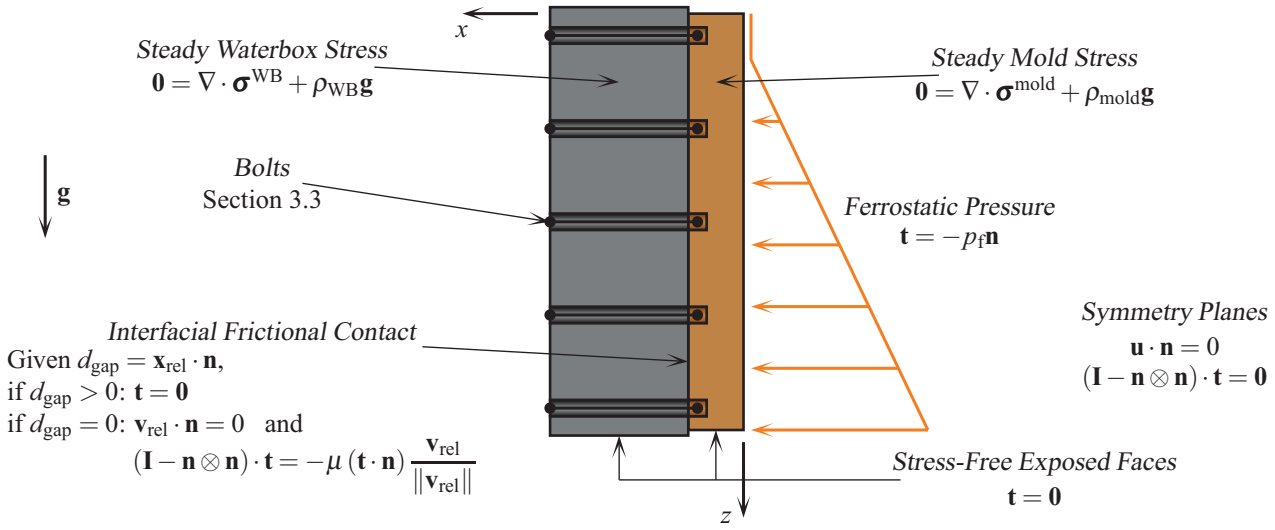

Figure 6. Boundary-value problem for mold plate, waterbox, and bolt displacement, strain, and stress fields

fixed in the direction of gravity. One point on the bottom of the waterbox arm is fixed in the direction of gravity to approximate the wide face resting on the oscillator. These constraints combined with the symmetry conditions prevent rigid-body motion of the assembly. The wide face stiffener stitch welds are modeled as constraint equations between several contacting points, on the tops and bottoms of the stiffeners to prevent rotation.

The strains are expected to be small: CON1D predicts a maximum mold temperature of about 300 °C, which causes a maximum thermal strain in the copper of about 4.5×10^{-3} m/m. The linearized strain-displacement relationship

$$\boldsymbol{\varepsilon} = \frac{1}{2}\left(\nabla\mathbf{u} + \nabla\mathbf{u}^{\mathrm{T}}\right), \tag{6}$$

where $\boldsymbol{\varepsilon}(\mathbf{x})$ is the total strain tensor field, therefore is adopted safely. The total strain rate tensor $\dot{\boldsymbol{\varepsilon}}$ additively decomposes into thermoelastic and inelastic parts as

$$\begin{aligned}\dot{\boldsymbol{\varepsilon}} &= \dot{\boldsymbol{\varepsilon}}^{\mathrm{te}} + \dot{\boldsymbol{\varepsilon}}^{\mathrm{ie}} \\ &= \left(\dot{\boldsymbol{\varepsilon}}^{\mathrm{el}} + \dot{\boldsymbol{\varepsilon}}^{\mathrm{th}}\right) + \left(\dot{\boldsymbol{\varepsilon}}^{\mathrm{pl}} + \dot{\boldsymbol{\varepsilon}}^{\mathrm{cr}}\right),\end{aligned} \tag{7}$$

where the thermoelastic strain rate $\dot{\boldsymbol{\varepsilon}}^{\mathrm{te}}$ decomposes into elastic $\dot{\boldsymbol{\varepsilon}}^{\mathrm{el}}$ and thermal $\dot{\boldsymbol{\varepsilon}}^{\mathrm{th}}$ parts, and the inleastic strain rate decomposes into a rate-independent plastic $\dot{\boldsymbol{\varepsilon}}^{\mathrm{pl}}$ and a rate-dependent creep $\dot{\boldsymbol{\varepsilon}}^{\mathrm{cr}}$ parts. This four-part strain decomposition has been used [10,12,14,15] to solve the problem efficiently during both short-time-scale events like startup and long-time-scale events like steady casting. If inelastic effects are neglected, then an additive decomposition of the thermoelastic strain is appropriate,

$$\boldsymbol{\varepsilon} = \boldsymbol{\varepsilon}^{\mathrm{el}} + \boldsymbol{\varepsilon}^{\mathrm{th}}, \tag{8}$$

as is done in this work.

Stress is related to elastic strain with Hooke's law,

$$\boldsymbol{\sigma} = \mathbb{C} : \boldsymbol{\varepsilon}^{\mathrm{el}}. \tag{9}$$

The components of the fourth-rank isotropic elastic stiffness tensor $\mathbb{C}(T)$ are

$$\mathbb{C}_{ijk\ell} = \frac{E}{2\,(1+\nu)}\left(\delta_{ik}\delta_{jl} + \delta_{i\ell}\delta_{kj}\right) + \frac{\nu E}{(1+\nu)\,(1-2\nu)}\delta_{ij}\delta_{k\ell}, \tag{10}$$

where $E(T)$ is Young's modulus, $\nu(T)$ is Poisson's ratio, and δ_{ij} is the Kroenecker delta (1 if $i = j$ and 0 otherwise). The elastic moduli of the coating layer have been modeled as isotropic and independent of temperature.[8] The constant values of the elastic moduli used in this work are given in Table I.

The thermal strain tensor $\boldsymbol{\varepsilon}^{\mathrm{th}}(\mathbf{x})$ is

$$\boldsymbol{\varepsilon}^{\mathrm{th}} = \alpha\,(T - T_{\mathrm{ref}})\,\mathbf{I}, \tag{11}$$

Table III. Details of bolt pre-stress calculations

Quantity	Symbol	Value		Unit
		Wide Face	*Narrow Face*	
Threads		M 20	M 12	
Pitch diameter	D_{pitch}	18.376	10.863	mm
Root diameter	D_{root}	17.294	10.106	mm
Thread angle	θ_{thread}	30	30	$^\circ$
Thread pitch	p_{thread}	2.5	1.75	mm
Thread coefficient of friction	μ_{thread}	0.16	0.16	–
Head mean diameter	D_{head}	34	15	mm
Head coefficient of friction	μ_{head}	0.6	0.6	–
Initial torque	τ_{bolt}	120	68	N·m
Initial axial force	F_{bolt}	9.746	11.74	kN
Initial axial stress	σ_{bolt}	61.32	103.77	MPa

where $\alpha(T)$ is the isotropic coefficient of thermal expansion (CTE) based on the strain-free reference temperature T_{ref}, and $\mathbf{I}$ is the second-rank identity tensor. In this work, the mold CTE is taken as the constant value given in Table I.

The operating shape of the waterbox is calculated reasonably well with an elastic model of the mold,[10] and the elastic predictions of mold shape shows qualitative agreement with measurements of a distorted mold after several heats.[3] Some model of inelastic effects is needed to predict residual distortion[3] and mold life.[15] Viscoplastic mold behavior is most appropriate because the mold operates at homologous temperatures of about 0.5 for several hours at a time.[15] Plastic models predict 3–4 times as much distortion as the elastic models,[1] and viscoplastic models predict larger strains than the plastic models.[15]

3.3. Mold Bolts

The array of bolts that hold the mold against the waterbox are key to controlling the distortion of the mold. The bolts have been modeled as prestressed bar elements[11,12] with point[12,13] and distributed[11] constraint equations to the mold and waterbox. Some authors have neglected the waterbox entirely, treating the bolt holes on the mold as zero total or zero normal displacement points or patches.[1,5,6,14,15] Other researchers include the waterbox and use constraint equations at the bolt locations.[8] Billet mold constraints have been modeled as pin constraints.[1,5–7]

In this work, the bolts that attach the mold to the waterbox are modeled as pre-stressed truss, *i.e.*, axial-extension–only, finite elements. The two nodes on the ends of the truss elements are connected to appropriate surfaces on the mold and waterbox, *i.e.*, the female threads on the mold and the bolt-head–bearing surfaces on the waterbox, using distributed constraint equations. These distributed constraint equations uniformly distribute the force on the controlling node over the nodes on the slave surface.

To convert the mold bolt into a pre-stressed truss element, each segment i of a bolt with cross sectional area A_i, length ℓ_i, and Young's modulus E_{bolt} is modeled as a spring with stiffness $K_i = A_i E_{\text{bolt}}/\ell_i$. The N segments of the bolt combine as springs in series, so each segment has the same force and the overall effective stiffness is $\frac{1}{K_{\text{eff}}} = \sum_{i=1}^{N} \frac{1}{K_i}$. The simulated bolt length ℓ_{bolt} is taken as the unstressed distance between the center of the female threads on the mold and the bolt-head–bearing surface on the waterbox, so the simulated cross-sectional area is $A_{\text{bolt}} = K_{\text{eff}}\ell_{\text{bolt}}/E_{\text{bolt}}$. The initial axial force F_{bolt} on the bolts is calculated[22,23] from the tightening torque τ_{bolt} as

$$F_{\text{bolt}} = \tau_{\text{bolt}} \Bigg/ \left(\frac{\mu_{\text{thread}}\pi D_{\text{pitch}} + \beta\, p_{\text{thread}}}{\beta\pi D_{\text{pitch}} - \mu_{\text{thread}} p_{\text{thread}}} \frac{D_{\text{pitch}}}{2} + \mu_{\text{head}} \frac{D_{\text{head}}}{2} \right), \tag{12}$$

where $\beta = \cos(\theta_{\text{thread}})$, p_{thread} and θ_{thread} are the pitch and angle of the threads, D_{pitch} is the pitch diameter of the threads, and μ_{thread} is the coefficient of friction between the male and female threads. Equation (12) also accounts for the effect of the tightening torque on the bolt head, which has not been done in previous work; in Equation (12), D_{head} is the mean diameter and μ_{head} is the coefficient of friction of the contacting annular region between the bolt head and bearing surface. The bolt force from Equation (12) is converted to a stress with $\sigma_{\text{bolt}} = F_{\text{bolt}}/A_{\text{bolt}}$. When post-processing the the calculated bolt behavior, the operating stress is returned to a force, and then this operating force is used to calculate the stress in each segment of the bolt, which is consistent with the springs-in-series model of the bolts used here. This treatment of the bolts slightly generalizes some previous work.[10,12]

3.4. Numerical Model Details

The mesh is a combination of fully-integrated linear tetrahera, wedges, and hexahedra: the ABAQUS element codes are DC3D4, DC3D6, and DC3D8 in the thermal model, and C3D4, C3D6, and C3D8 in the mechanical model. The mold bolts are axial-extension only T3D2 linear truss elements. The complete assembly consists of 1 032 210 nodes and 1 414 927 elements. The thermal analysis required 115 s to solve the 291 447-equation system, and the mechanical analysis required 53.3 h to solve iteratively the 3 206 919-equation system, both on a 6-core 2.66 GHz Intel Xeon processor with 48 GB of RAM.

The "hard" contact algorithm was employed to treat the interfacial behavior between the "master" mold and "slave" waterbox surfaces, and between the "master" narrow face and "slave" wide face surfaces. To aid convergence, a solver-determined viscous damping coefficient artificially dissipates some energy, but a simulation was accepted only if the ratio of the dissipated energy to the total strain energy was less than 5%. This non-linear model was marched through pseudo-time, applying successively larger increments of the temperature change and converging at intermediate mechanical states. Across the model development process, experience revealed that an initial load fraction of 0.0075 minimized number of the global Newton iterations in the first step at 13. The largest load fraction permitted was 0.1 to avoid excessive iterations or divergence, and a typical simulation required a total of 16 load increments and 119 global iterations.

4. THERMAL MODEL RESULTS

The calculated temperatures for the hot face and a typical channel root are shown in Figures 7 and 8 for the wide face and narrow face molds. The highest hot face temperatures, 390 °C on the WF and 430 °C on the NF, were found about 35 mm below the meniscus. The narrow face generally is hotter than the wide face because its hot face to channel root distance is 5 mm larger than on the wide face. Below the peak, the hot face temperature monotonically decreases with increasing distance down the mold until the last approximately 50 mm, where the water channels curve out to the back of the mold and into the waterbox. The WF hot face temperature increases by 7.8 °C to 18.4 °C near the locations of the bolt and thermocouple holes because of the cooling channel slaloms around these features; this observed increase is about 4.5% higher than the average hot face temperature

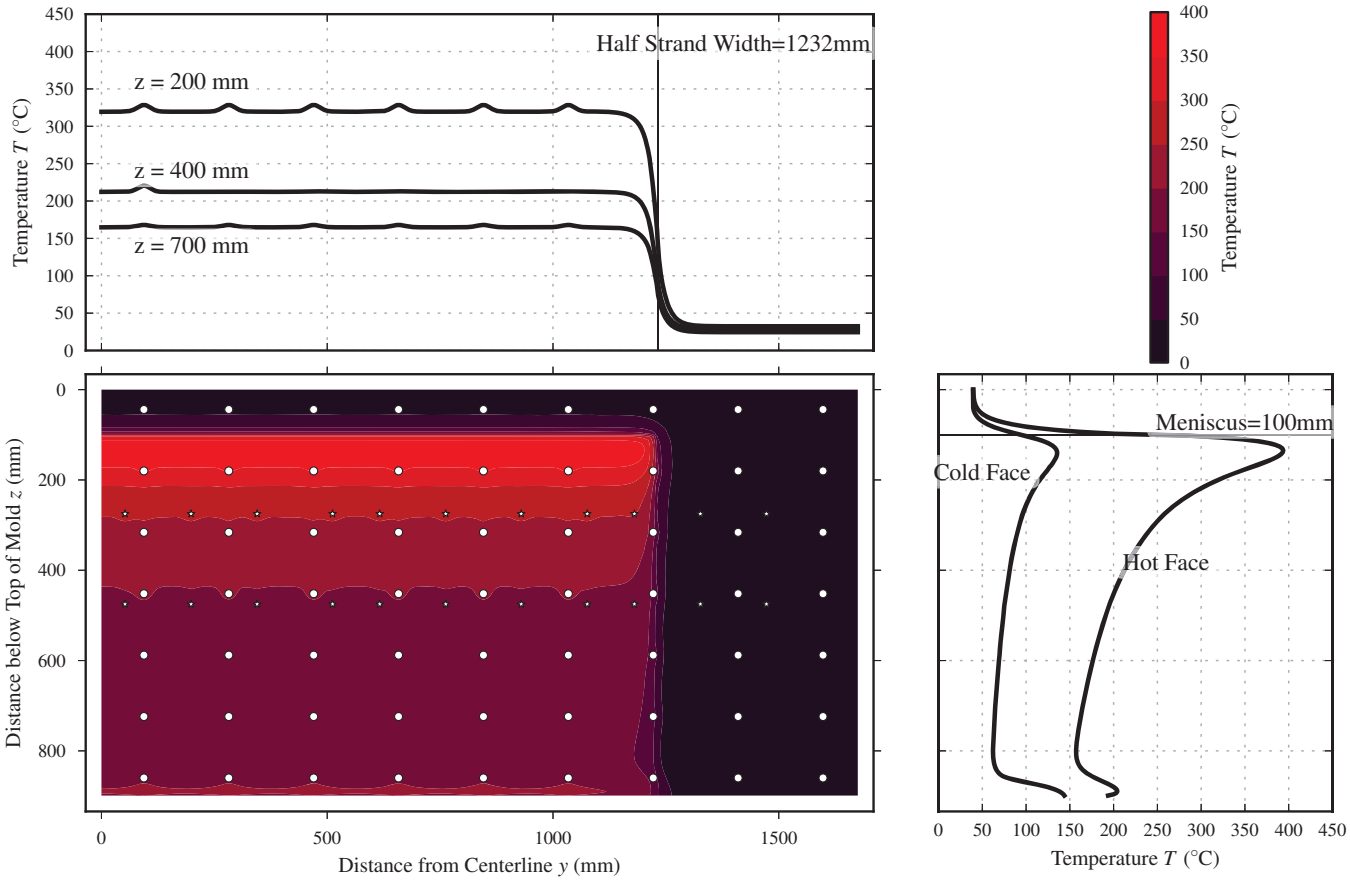

Figure 7. Wide face temperatures

between bolt holes, and the temperature increases span about 25 mm on either side of the bolt hole, which is about the distance to the root of the adjacent channel. This "bolt effect" is not as pronounced on the NF because the plate is so narrow, and because of the bore in the corners. The bored cyindrical water channel near the corners of the narrow face cools the mold well: the corner of the hot face is about 75 °C cooler than the centerline at the peak temperature 35 mm below meniscus, and this difference is about 25 °C at the bottom of the mold.

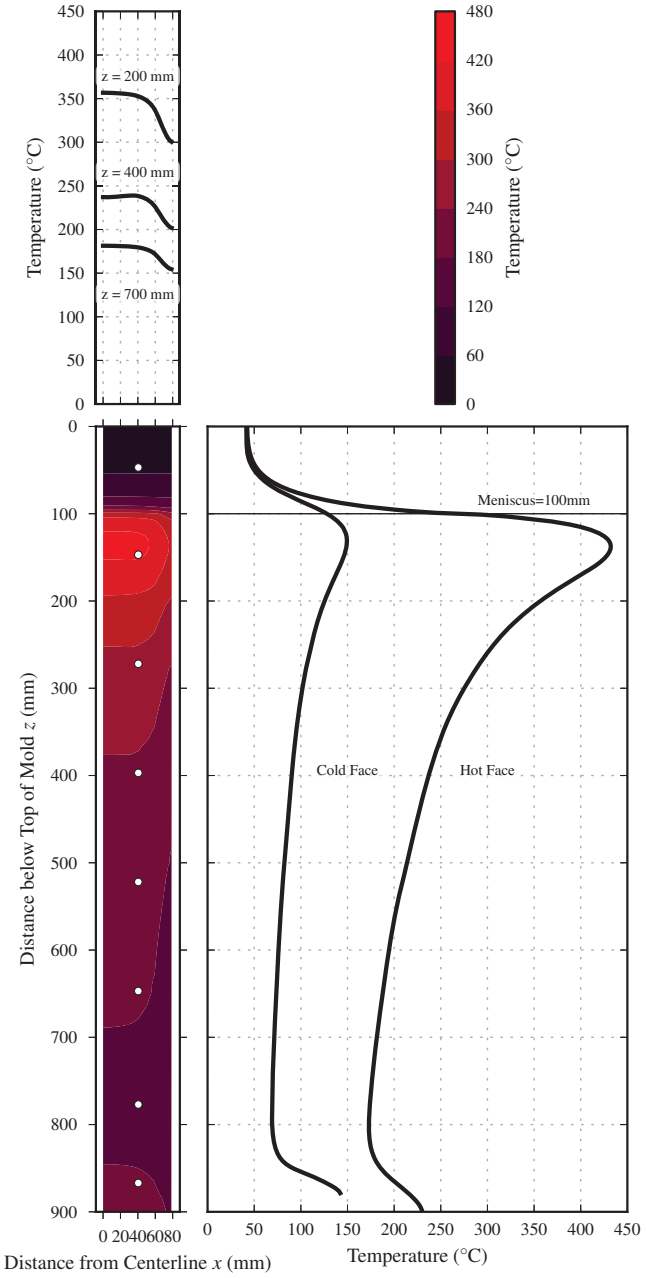

Figure 8. Narrow face temperatures

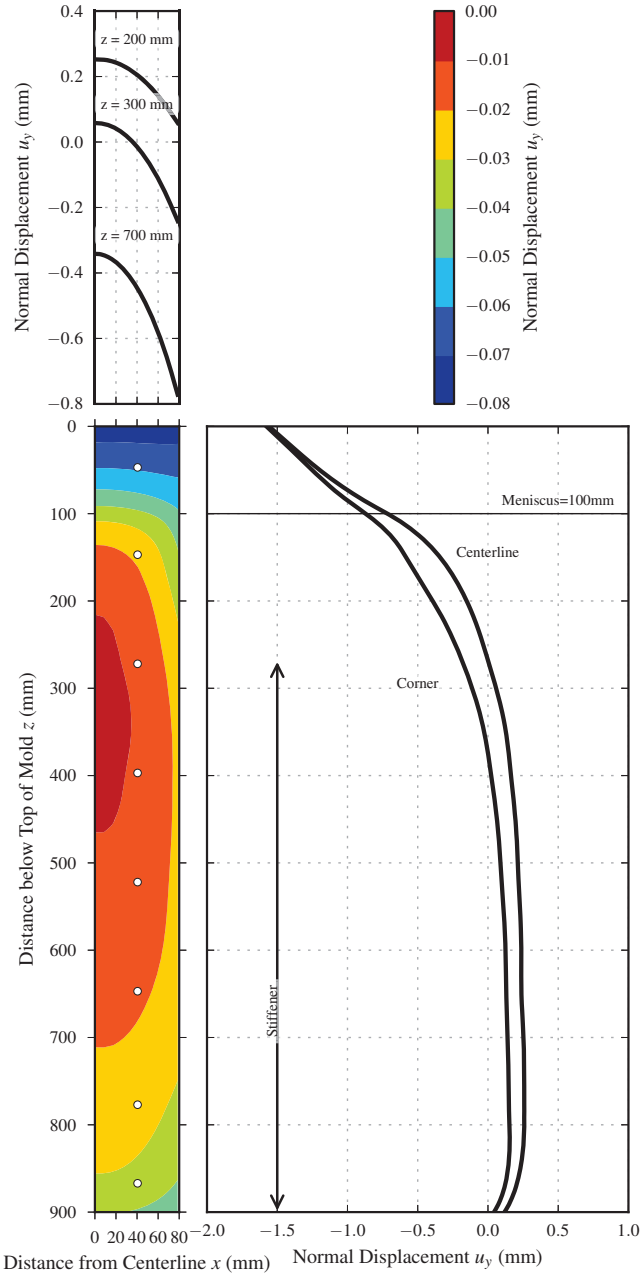

Figure 9. Narrow face distortion

5. MECHANICAL MODEL RESULTS

The calculated hot face distortion profiles in the normal direction are shown in Figures 9 and 10 for the narrow face and wide face molds. The upper part of the NF mold bends away from the strand, while the lower part of the NF shows almost no distortion, due to the stiffener plate on the back of the waterbox. Superimposed with this bulk behavior, the NF plate bends convex into the strand, *i.e.*, the centerline is closer to the SEN than the corners, by about 0.35 mm. The maximum distortion of the wide face mold is 0.24 mm into the strand at about 70 mm below the meniscus at its centerline, as shown in Figure 10. The wide face curls such that the edges push into the water box and the center pushes into the strand. The bolts keep the mold attached to the

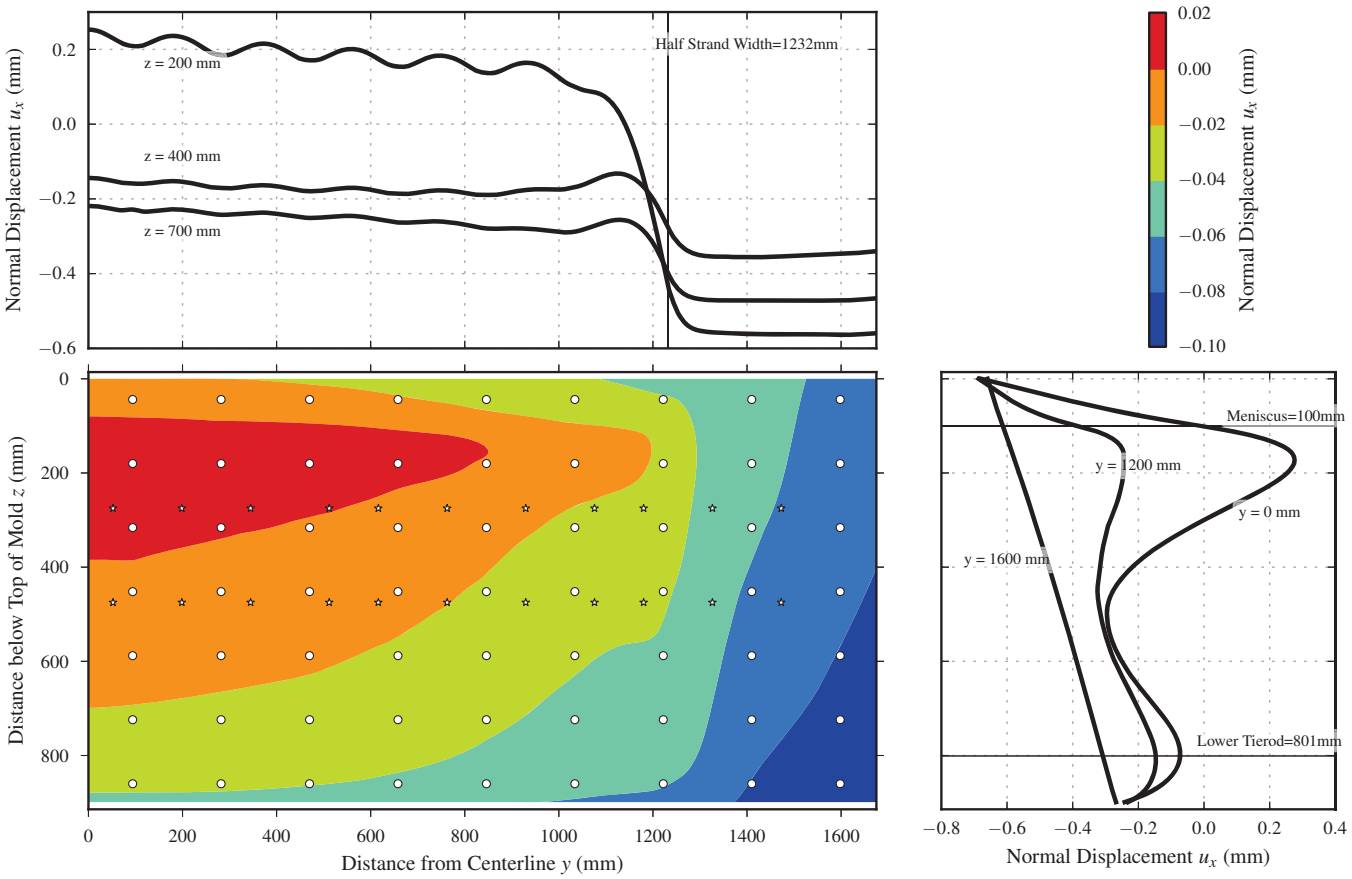

Figure 10. Wide face distortion

waterbox, and also locally restrain the distortion, as seen by the distortion profiles in Figure 10. Looking down the length of the mold, the distortion profile has a peak about 70 mm below the meniscus and another peak about 100 mm above mold exit; the higher peak certainly is driven by the highest temperatures in the mold, but both peaks are coincident with the water header boxes at the top and bottom of the waterbox, which are more flexible than the rigidly-supported middle region. The severity of these peaks decreases with increasing distance from the centerline, to none past the strand width. For both the WF and NF molds, the peak distortion occurs lower in the mold than the peak temperature.

This mold has less distortion than those analyzed in previous work because of the stiffeners oriented perpendicular to the back of the waterboxes, and overall stiffer construction. The stiffener plate on the NF waterbox is particularly effective at preventing distortion, keeping the distortion around 0.2 mm in the lower part of the mold. The about 1 mm of distortion near the meniscus, above this stiffener plate, is beneficial because it adds curvature that contributes to NF taper.

The wide face and narrow face molds contact in two locations, as seen in Figure 11, near 190 mm below the top of the mold and near mold exit. The gap between the narrow face and wide face is a maximum of 0.12 mm about 500 mm below the top of the mold. Figure 12 show top-view slices through the assembly at 190 mm below top of mold; at this eleveation most of the wide face is not in contact with its waterbox, and the molds are in contact only at the NF corner, opening a wedge-shaped gap between them. Similar gap behavior has been observed in previous studies.[10,11] Excessive clamping force can crush the NF corners and cause fin defects, as discussed in Section 1.4, but owing to the stiff construction and careful filling practice used for this mold, this mold no longer has issues with corner fins and related breakouts.

6. CONCLUSIONS

This work explored the thermal and mechanical behavior of a wide slab-casting mold. The water channel slaloms around bolt and thermocouples cause a small but localized increase in hot face temperature, and the change in cooling near mold exit causes a much more substatial increase in hot face temperature. The wide face mold distorts into a W-shape because of the peak temperature near the meniscus and the lower waterbox stiffness near mold exit. The narrow face mold remains flat in the lower part of the mold because of a stiffener plate on the waterbox, and curves away from the solidifying steel above the stiffener. This

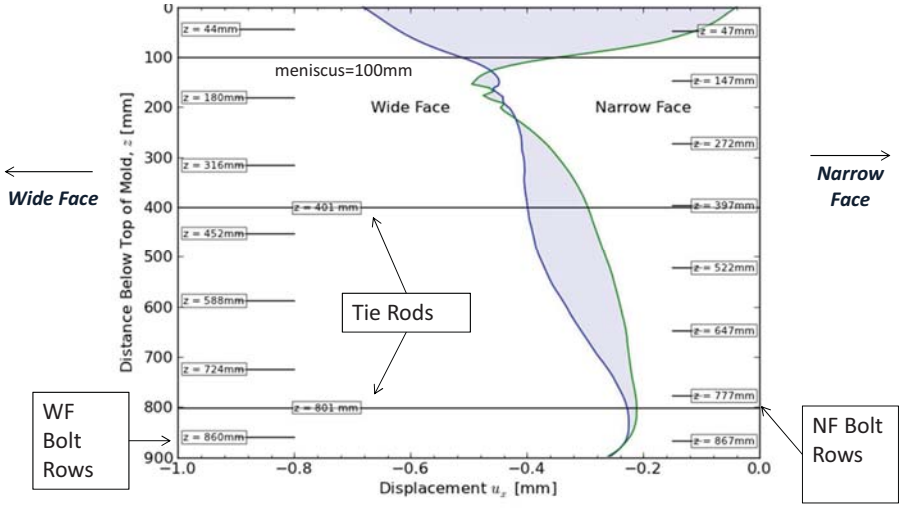

Figure 11. Wide Face Narrow Face Interface

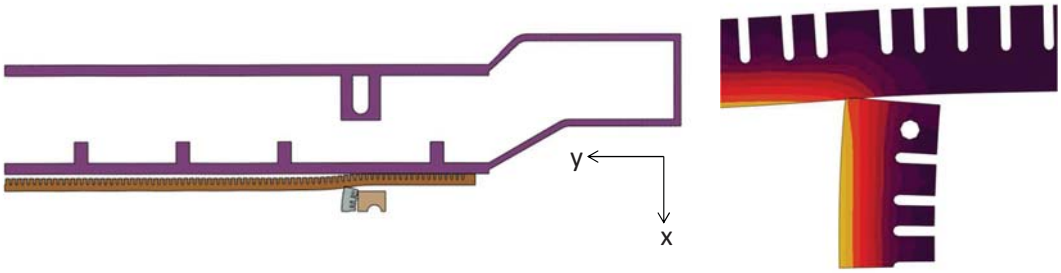

Figure 12. Top View of Entire Mold 190 mm below Top and Close Up Near Corner

mold waterbox design features very stiff reinforcement, which is necessary for the wide slabs cast in it.

ACKNOWLEDGMENTS

The financial support of the members of the Continuous Casting Consortium at the University of Illinois at Urbana–Champaign is acknowledged gratefully. At the time of writing, the members are: ABB, ArcelorMittal, Baosteel, Magnesita Refractories, Nippon Steel and Sumitomo Metal Corporation, Nucor Steel Decatur, POSTECH/POSCO, SSAB, and ANSYS-FLUENT. The authors also thank the researchers and plant personnel at the undisclosed sponsoring company for measurements from the plant.

REFERENCES

1. I. V. Samarasekera, D. L. Anderson, and J. K. Brimacombe, "The thermal distortion of continuous-casting billet molds," *Metallurgical Transactions B*, vol. 13, no. 1, pp. 91–104, 1982.
2. M. Ansoldi, G. Bazzaro, D. Benasciutti, F. D. Bona, G. Luvarà, L. Moro, M. G. Munteanu, and F. Vecchiet, "Thermo-mechanical analysis of a copper mould for continuous casting of steel," *Integritet i vek konstrukcija*, vol. 13, no. 1, pp. 29–36, 2013.
3. H. Gravemann, "Mould tubes with improved service life for continuous casting of steel," in *Proceedings of Continuous Casting '85*, The Institute of Metals, 1985. Paper 20.
4. V. Krujelskis and J. Cook, "The influence of mould tube taper and distortion on cast billet quality," in *Proceedings of the 71st Steelmaking Conference*, pp. 349–352, The Iron and Steel Society, 1988.
5. J. E. Kelly, K. P. Michalek, T. G. O'Connor, B. G. Thomas, and J. A. Dantzig, "Initial development of thermal and stress fields in continuously cast steel billets," *Metallurgical Transactions A*, vol. 19, no. 10, pp. 2589–2602, 1988.

6. J.-E. Lee, H. N. Han, K. H. Oh, and J.-K. Yoon, "A fully coupled analysis of fluid flow, heat transfer and stress in continuous round billet casting," *ISIJ International*, vol. 39, no. 5, pp. 435–444, 1999.
7. H. Yin, M. Yao, H. Zhan, and D. Fang, "3D stress model with friction in and of mould for round billet continuous casting," *ISIJ International*, vol. 46, no. 4, pp. 546–552, 2006.
8. X. Liu and M. Zhu, "Finite element analysis of thermal and mechanical behavior in a slab continuous casting mold," *ISIJ International*, vol. 46, no. 11, pp. 1652–1659, 2006.
9. D. M. Salkiewicz, J. O. Ratka, B. D. Horn, and R. P. Natili, "Development and performance results – high performance copper alloy for continuous slab casting molds," in *Proceedings of the 78th Steelmaking Conference*, pp. 369–376, The Iron and Steel Society, 1995.
10. B. G. Thomas, G. Li, A. Moitra, and D. Habing, "Analysis of thermal and mechanical behavior of copper molds during continuous casting of steel slabs," *Iron and Steelmaker (ISS Transactions)*, vol. 25, no. 10, pp. 125–143, 1998.
11. L. C. Hibbeler, B. G. Thomas, R. C. Schimmel, and G. Abbel, "The thermal distortion of a funnel mold," *Metallurgical and Materials Transactions B*, vol. 43, no. 5, pp. 1156–1172, 2012.
12. J. K. Park, B. G. Thomas, I. V. Samarasekera, and U. S. Yoon, "Thermal and mechanical behavior of copper molds during thin-slab casting (I): Plant trial and mathematical modeling," *Metallurgical and Materials Transactions B*, vol. 33, no. 3, pp. 425–436, 2002.
13. U.-S. Yoon, J. K. Park, B. G. Thomas, and I. Samarasekera, "Mold crack formation of the funnel shaped mold during thin slab casting," in *Proceedings of the 85th Steelmaking Conference*, pp. 245–257, The Iron and Steel Society, 2002.
14. W. Luo, B. Yan, X. Lu, and G. H. Wen, "Improvement of water slot design for beam blank casting mould," *Ironmaking and Steelmaking*, vol. 40, no. 8, pp. 582–589, 2013.
15. T. G. O'Connor and J. A. Dantzig, "Modeling the thin-slab continuous-casting mold," *Metallurgical and Materials Transactions B*, vol. 25, no. 3, pp. 443–457, 1994.
16. C. G. Dilnot, G. Hugenschütt, D. Rode, and H.-G. Wobker, "Slab quality and mold wear in continuous casting," in *Proceedings of the 6th European Conference on Continuous Casting*, Associazione Italiana di Metallurgia, 2008.
17. K. Tada, S. Kasai, A. Ichihara, and H. Onishi, "Improvement in service life of continuous casting mold," *Kawasaki Steel Technical Report*, vol. 17, pp. 26–33, 1987.
18. B. G. Thomas, J. Jiang, and D. Lorento, "Optimization of water channel design in beam-blank molds," in *Proc. 5th Eur. Conf. Contin. Cast.*, pp. 139–147, The Institute of Materials, Minerals, and Mining, 2005.
19. J. K. Park, B. G. Thomas, I. V. Samarasekera, and U. S. Yoon, "Thermal and mechanical behavior of copper molds during thin-slab casting (II): Mold crack formation," *Metallurgical and Materials Transactions B*, vol. 33, no. 3, pp. 437–449, 2002.
20. I. V. Samarasekera and J. K. Brimacombe, "The thermal field in continuous-casting molds," *Canadian Metallurgical Quarterly*, vol. 18, no. 3, pp. 251–266, 1979.
21. Y. Meng and B. G. Thomas, "Heat-transfer and solidification model of continuous slab casting: CON1D," *Metallurgical and Materials Transactions B*, vol. 34, no. 5, pp. 685–705, 2003.
22. R. C. Juvinall and K. M. Marshek, *Fundamentals of Machine Component Design*, ch. 10. John Wiley & Sons, 3rd ed., 2000.
23. J. E. Shigley and C. R. Mischke, *Standard Handbook of Machine Design*, ch. 20.3. McGraw-Hill, 2nd ed., 1996.